

Evaluation of the region 1 field-aligned current from the low-latitude boundary layer using the 1989 Tsyganenko model

Takashi Yamamoto¹, Masao Ozaki² and Shoshi Inoue³

¹*Department of Earth and Planetary Science, University of Tokyo, 3-1,
Hongo 7-chome, Bunkyo-ku, Tokyo 113-0033*

²*Institute of Industrial Science, University of Tokyo, 6-1, Komaba 4-chome,
Meguro-ku, Tokyo 153-8505*

³*Faculty of Education, Iwate University, Morioka, Iwate 020-8550*

Abstract: On the basis of the 1989 Tsyganenko magnetic field model, the field-aligned current (FAC) density distribution in the low-latitude boundary layer (LLBL) is numerically evaluated by assuming the entry of magnetosheath particles into the LLBL. The calculated FAC density/intensity profiles are consistent with observations. This FAC generation arises from the divergence of the magnetic drift current density carried by LLBL particles, and the current intensity is then increased with their kinetic energy density. The FAC generation occurs at the inner edge of the LLBL whenever sheath particles penetrate into the magnetosphere, regardless of the entry process. It is also emphasized that the LLBL FAC production is an inevitable consequence of the formation of the magnetopause, because the magnetopause currents act to shield the magnetic field originating from the currents inside the closed region of the magnetosphere, causing the LLBL inner edge to intersect the magnetic drift paths. This simple situation can be illustrated by calculating the distribution of the flux tube volume in the Tsyganenko model.

1. Introduction

Previously, the region 1 current was thought to be connected to a single topological region in the magnetosphere. Using ground-based magnetometer chain measurements, however, Friis-Christensen and Lassen (1991) suggested that the region 1 current actually consists of two separate regions, one (region 1a) connected to the low-latitude boundary layer (LLBL) and one (region 1b) connected to the plasma sheet. Simultaneous particle and magnetic field measurements have shown that the region 1a FAC can be subdivided into the cusp and LLBL parts (Newell *et al.*, 1991; Yamauchi *et al.*, 1993). Moreover, careful observations have established that plasma particles in the LLBL are responsible for the generation of a major portion of the dayside region 1 field-aligned current (FAC) (*e.g.*, Bythrow *et al.*, 1981, 1988; Newell *et al.*, 1991; Woch and Lundin, 1993), while a portion of it may be sustained by particles in the plasma sheet (*e.g.*, Liou *et al.*, 1999).

The viscous interaction between the solar wind and the magnetospheric plasma (Axford and Hines, 1961) had long been believed to be the most likely mechanism for the

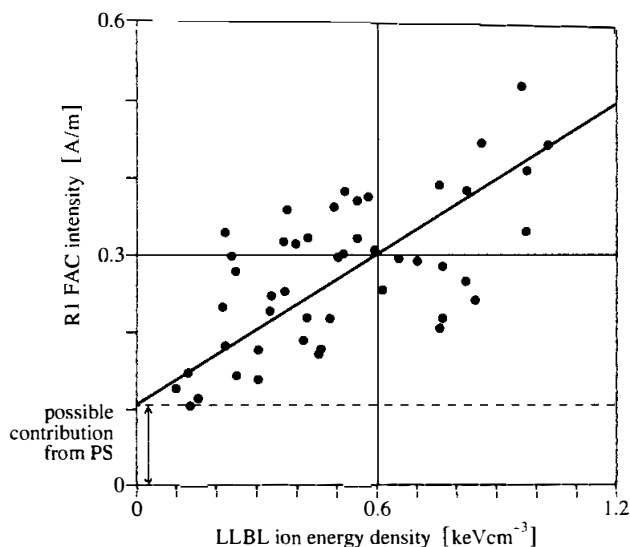


Fig. 1. Region 1 FAC intensity versus the energy density of the LLBL ion population, in northward IMF conditions. The full line represents a linear fit to the data points. This figure is adapted from Fig. 4 of Woch *et al.* (1993).

FAC generation in the LLBL. The viscous interaction model assumes that the sheared plasma flow in the LLBL produces negative and positive space charges in the postnoon and prenoon sectors, respectively. Coupling to the ionosphere might produce FAC flows away from the polar ionosphere to the boundary layer in the postnoon sector and vice versa in the prenoon sector (*e.g.*, Sonnerup, 1980; Lotko *et al.*, 1987). In a simple model by Sonnerup, the FAC density (intensity) is proportional to the plasma bulk flow speed in the magnetosheath. On the other hand, Yang *et al.* (1994) proposed a theoretical model for the pressure-gradient-driven FACs in the LLBL. Moreover, Yamamoto *et al.* (1995) has shown that the required (for FAC generation) inclination of the gradient/curvature drift direction relative to the LLBL inner edge, as was predicted by Yang *et al.*, actually exists in the LLBL region of the Tsyganenko (1989) magnetic field model (hereafter referred to as T89). This fact supports the pressure-gradient-driven mechanism for the generation of LLBL FACs. A number of observations favor the pressure-driven mechanism rather than the viscous interaction model, and this point will be discussed in the subsequent review of LLBL current/particle observations.

Iijima and Potemra (1982) examined the relationship between hourly values of the solar wind density, speed and the interplanetary magnetic field (IMF) and the densities of region 1 FACs in the dayside (0800–1600) MLT sectors. The correlation between the current density and the solar wind speed was shown to be poor, suggesting that the viscous interaction is not likely to play a major role in the LLBL FAC generation. The observation by the Viking satellite (Woch *et al.*, 1993) showed that under northward IMF conditions, the region 1 FAC intensity in the 0400–1030 MLT range is positively correlated with the LLBL ion energy density. Figure 4 of their paper is reproduced as Fig. 1 in the present paper. Assuming that a possible contribution from the plasma sheet to the current intensity is represented by an intercept of the regression line fitted to the data points, the

FAC intensity solely from the LLBL is inferred to be directly proportional to the LLBL ion energy density. This observation then supports the pressure-driven mechanism for the LLBL FAC generation.

Furthermore, Viking observations (Potemra *et al.*, 1987; Bythrow *et al.*, 1987) have revealed a close relation between LLBL particles and FACs, namely that an intense region 1 current localized in an extremely narrow ($<0.1^\circ$ in invariant latitude) zone is seen near the inner (equatorward) edge of the LLBL particle population. Plate 1 of Potemra *et al.* and Fig. 2 of Bythrow *et al.* are reproduced as Figs. 2 and 3 in the present paper, respectively. Figure 3 is to notify that such a fine current structure cannot be identified by measurements from the low-altitude satellite DMSP, owing to their low spatial resolution

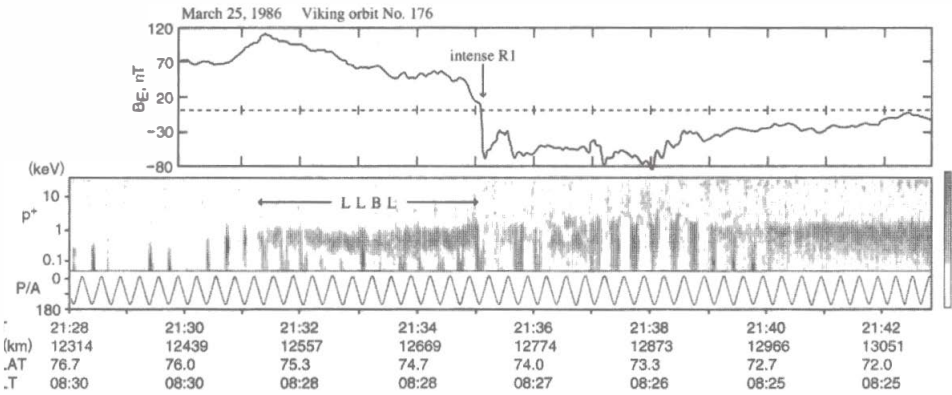


Fig. 2. Viking observations of the east-west component of the magnetic field (top), the energy-time spectrogram of positive ions (bottom), and the particle pitch angle with 0° denoting precipitating particles (very bottom) (adapted from Plate 1 of Potemra *et al.* (1987)). The ion spectrogram also shows ion conics characterized by the “tuning fork” signatures (Gurgiolo and Burch, 1982) beginning at about 2131:30 UT.

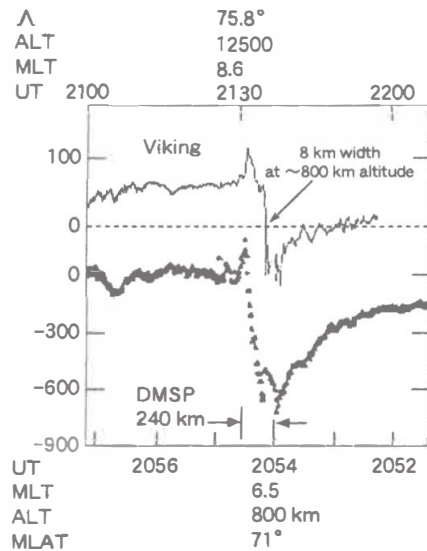


Fig. 3. Magnetic field traces from the Viking (top) and DMSP-F7 (bottom) satellites for the same event as Fig. 2 (adapted from Fig. 2 of Bythrow *et al.* (1987)). The spatial resolution (in invariant latitude) of the Viking data is one order of magnitude higher than the DMSP data.

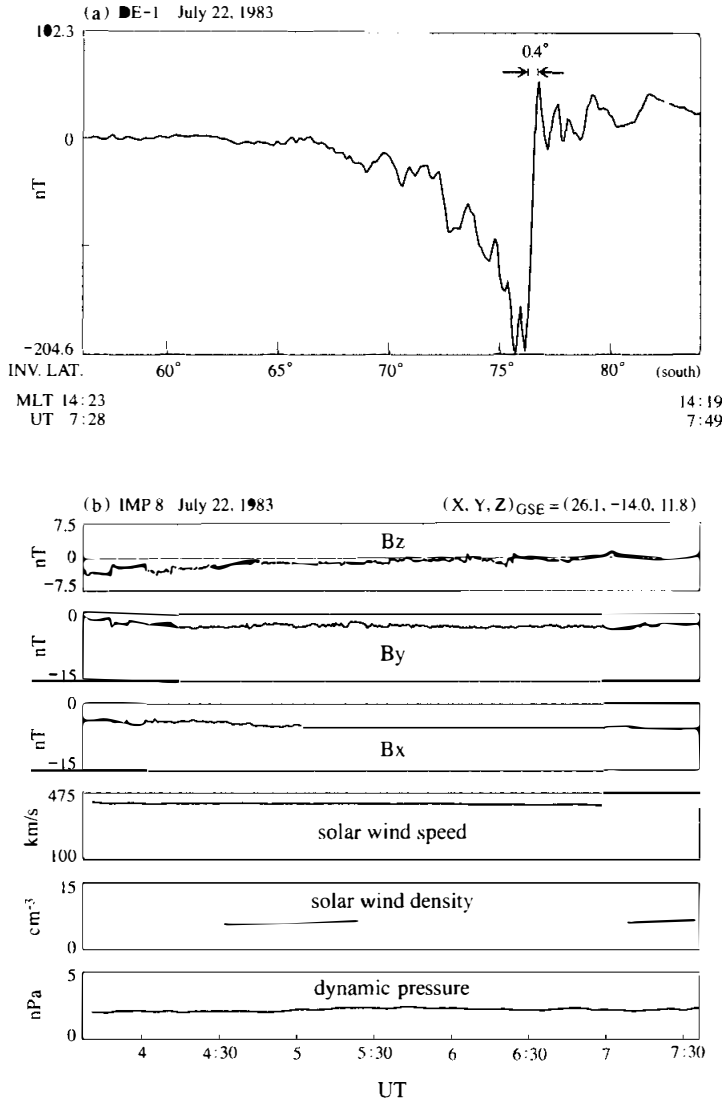


Fig. 4. (a) Example of (6s average) data of east-west magnetic field in the LLBL, measured from the DE-1 satellite, showing that the total region 1 current intensity is substantially maintained by an (apparently) single current sheet of narrow width. The magnetic field is calibrated to that at an altitude of 800 km. The spatial resolution of this data is about 0.1° in invariant latitude. (b) Variations of the IMF GSM components as well as the solar wind speed, density and dynamic pressure, which were all 5-min averages and measured from the IMP 8 satellite for a four-hour period just prior to the DE-1 observation of the current structure in (a).

(although these observations from the two spacecraft were not at the same universal and local times.) In the current system in Fig. 2 or 3, downward (region 1) currents with even smaller densities can also be seen inside the region of LLBL particle population, contributing to the total region 1 current intensity. Cases that the total region 1 current intensity

is substantially maintained by an (apparently) single current sheet of narrow width can be found in the (6-s average) data of magnetic field perturbations measured from the Dynamics Explorer-1 (DE-1) satellite. An example of such a current structure in the LLBL is shown in Fig. 4a. The width of the region 1 current is about 0.4° in invariant latitude, even narrower than its average value of $1\text{--}2^\circ$ (Iijima and Potemra, 1978). Simultaneous particle data is not available for this particular case. For one other case of a similar current structure (the search for such current structures is ongoing), the current region is found to be roughly collocated with the LLBL inner edge, although the resolution of available particle data is about 1° . Needless to say, such a spatial relation between the region 1 FAC and the LLBL inner edge is just a prediction from the pressure-gradient-driven model. Note that Lotko and Sonnerup (1995) have opposed this model, partly because FACs generated in the pressure-driven model would flow in δ -function sheets at the inner edge of a crosswise-uniform (LLBL) layer. As shown in Figs. 2 and 4a, however, the FAC does occasionally flow in a δ -function-like sheet. Notably, the region 1 current with an average width of $1\text{--}2^\circ$ has been commonly categorized as the large-scale one, but it sometimes exhibits a signature of localization to a narrow ($<0.5^\circ$) latitudinal zone. (For such examples for the nightside region 1 currents, see Yamamoto *et al.* (1999)). While physical reasons for the variations in LLBL FAC width will be discussed in Section 5, a precondition for the appearance of a single region 1 current structure of narrow width is assumed to be steadiness of the solar wind, *i.e.*, steady solar wind speed, density and magnetic field. In general, a simplest current structure created in a steady environment surrounding the magnetosphere is expected to provide a clue to the FAC generation mechanism.

The purpose of the present paper is to numerically evaluate the LLBL FAC density/intensity using the T89 magnetic field model, assuming that magnetosheath particles penetrate into the closed magnetosphere to form the LLBL. Importantly, the charge separation responsible for the FAC generation necessarily occurs in the LLBL, which can be intuitively understood from illustration of the direction of average magnetic drift (gradient B drift plus curvature drift) velocity of particles. Conditions that control the thickness (in latitude) of an FAC zone in the LLBL will also be discussed.

2. Model of LLBL

In this section, a simple model of the low-latitude boundary layer is presented on the basis of the T89 model. The $K_\rho=0$ version of T89 with a nontilted geodipole is used throughout this work unless otherwise stated. While the Tsyganenko models have been used to describe the magnetic field distribution, various plasma regimes such as the LLBL and the plasma sheet, observationally distinguished in the magnetosphere, are not specified in them. In general, those plasma regimes in the Tsyganenko models may then be identified by comparing the ionospheric foot points of their field lines with the distributions of precipitating particles observed from low-altitude satellites. Since the LLBL is adjacent to the magnetopause, the latter should first be determined in T89. According to Kaufmann *et al.* (1993), the magnetopause (in T89) is defined as the outer boundary of all the closed field lines. (To describe the LLBL, the open-closed boundary crossing the distant tail need not be determined.) To conform with the precipitation patterns of LLBL

particles, statistically determined by Newell and Meng (1994), the inner edge of the LLBL in T89 is defined, on the equatorial plane, as follows. The distance, \mathcal{L} (in units of the Earth's radius, R_E), between a point on the inner edge and the magnetopause boundary is given by

$$\mathcal{L}(X) = 0.25 \cdot (2 - X/X_{\text{sub}}), \quad \text{for } 0 \leq X \leq X_{\text{sub}} \quad (1)$$

$$\mathcal{L}(X) = 0.5, \quad \text{for } X \leq 0 \quad (2)$$

where the X -coordinate is specified on the magnetopause, and X_{sub} is for the subsolar point on it. (In this paper, the solar-magnetospheric coordinates (X, Y, Z) are used.) This profile is consistent with a finding by Mitchell *et al.* (1987) that the thickness of the LLBL tends to increase with distance from the subsolar point. Figure 5a shows the magnetopause boundary and the above-defined LLBL inner edge on the equatorial plane. (Due to the symmetry of the model field with respect to the X - Z plane, various quantities are only shown on the duskside, except in Fig. 7, while the region 1 FAC direction is reversed on the dawnside.) The ionospheric projection of the LLBL inner edge is shown in Fig. 5b. Also indicated are 'division lines', each of which divides the LLBL region according to its relative (to \mathcal{L}) distance from the magnetopause. For example, 1/2 line is located at a distance of $\mathcal{L}(X)/2$ from the magnetopause. In T89, the ionospheric projection of the magnetopause (defined as the open/closed boundary) seems to converge to a single point or a short line segment as the computational resolution is increased sufficiently. Namely, in this model the dayside cusp, if defined to be a region of open field lines, has ionospheric projection of negligible dimension. In the present analysis, the 'near-cusp' region is formally defined, on the equatorial plane, to be a region between 1/32 line and the magnetopause boundary. The generation of FACs in the open cusp region (*e.g.*, Erlandson *et al.*, 1988; Taguchi *et al.*, 1993; Yamauchi *et al.*, 1993) is beyond the scope of the present paper.

Next, the particle (energy) distribution in the LLBL region is modeled. To this end, the orthogonal curvilinear coordinates (ξ, η) on the equatorial plane are introduced as illustrated in Fig. 5a. The ξ -axis is taken to be the magnetopause boundary; the ξ -distance is measured from the subsolar point. The η -axis is locally (at a given ξ) defined to be perpendicular to the ξ -axis and directed inward; the η -distance is measured from the ξ -axis, *i.e.*, the magnetopause boundary, and it is normalized by the LLBL thickness $\mathcal{L}(\xi)$. The particle (energy) distribution is given in terms of the flux tube energy content, ε , which is defined as the total kinetic energy of plasma particles contained in a flux tube with unit cross-sectional area at the ionospheric height:

$$\varepsilon \equiv \int_{s_i}^{s_e} \frac{3p}{2} \frac{B_i}{B(s)} ds, \quad (3)$$

where p is the isotropic plasma pressure, s is the field-aligned distance, and s_e and s_i are the distances to the equator and the ionospheric height, respectively; $B(s)$ and B_i are the magnetic field intensities at distances s and s_i , respectively. Assuming that the average energies of protons and electrons, W^p and W^e , are constant along field lines, ε is written as

$$\varepsilon = (W^p + W^e)N, \quad (4)$$

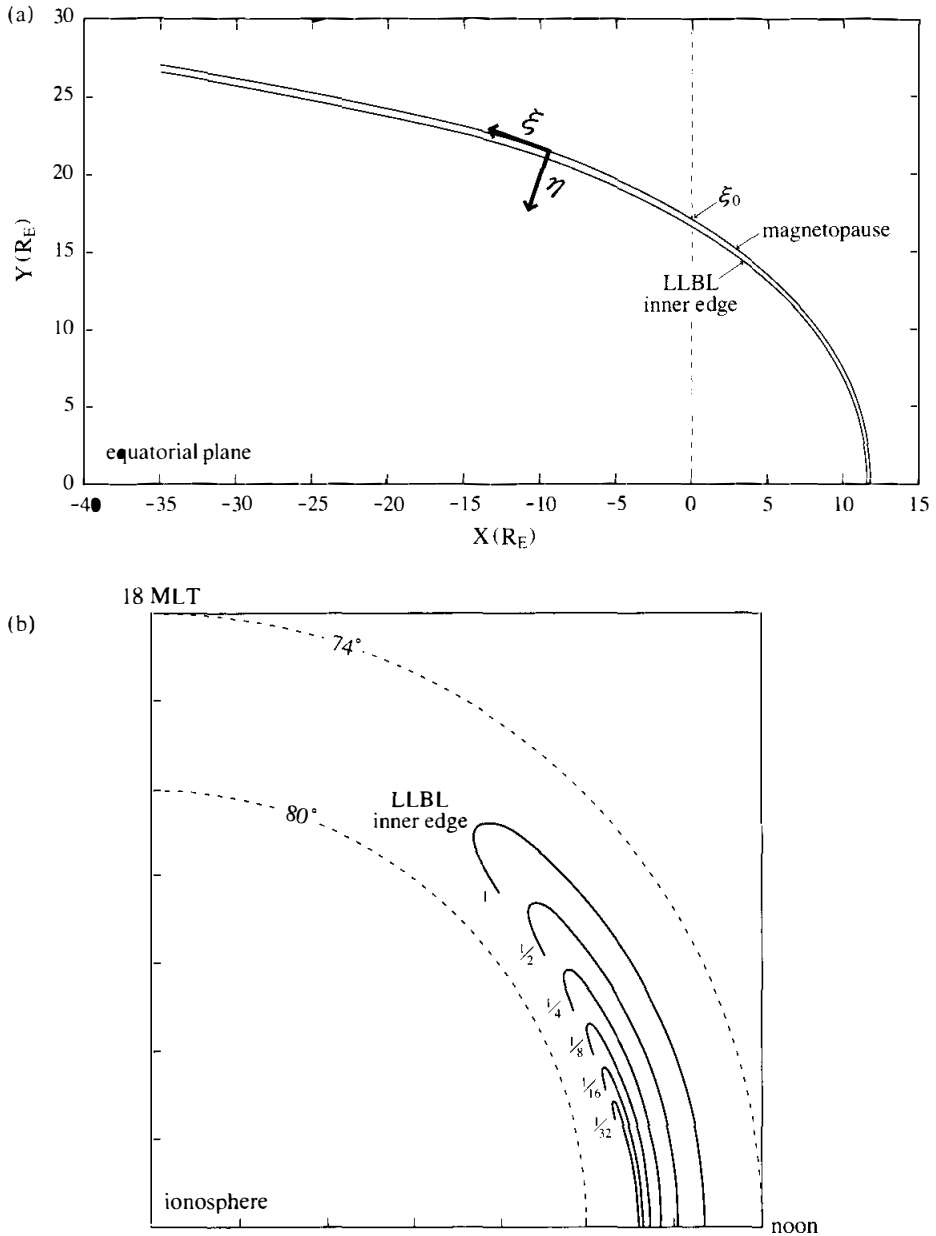


Fig. 5. (a) Magnetopause boundary and LLBL inner edge on the equatorial plane, which are defined, using T89, in Section 2. The ξ - and η -axes are indicated. (b) Solid curves labeled 1, $1/2$, $1/4$, $1/8$, $1/16$ and $1/32$ show the ionspheric projections of the division lines at $\eta = 1, 1/2, 1/4, 1/8, 1/16$ and $1/32$ on the equatorial plane, respectively. The tailward limits of these lines are determined from the condition that the adiabaticity parameter, κ , is equal to unity. (For an explanation of this condition, see Section 3.)

where N is the flux tube content defined as follows:

$$N \equiv \int_{s_i}^{s_r} n \frac{B_i}{B(s)} ds, \quad (5)$$

where n is the number density of protons or electrons. This equation means that N is the number of particles in a flux tube with unit (ionospheric) cross section. If n is constant along field lines, N is written as nR_b , where R_b is the flux tube volume defined as

$$R_b \equiv \int_{s_i}^{s_r} \frac{B_i}{B(s)} ds. \quad (6)$$

The model distribution of ε in the LLBL regions is expressed as a function of ξ and η :

$$\varepsilon = \varepsilon_0 f(\xi) g(\eta), \quad (7)$$

$$f(\xi) = \{R_b(\xi)/R_b(\xi_0)\}^\gamma, \quad (8)$$

$$g(\eta) = 1, \quad \text{for } 0.0 \leq \eta \leq \eta_0 \quad (9)$$

$$g(\eta) = \frac{1}{a} \left\{ b - \tanh\left(\frac{\eta - 1/2}{\delta\eta}\right) \right\}, \quad \text{for } \eta_0 \leq \eta \leq 1.0 \quad (10)$$

where η_0 is fixed at $1/32$. In eq. (8), $R_b(\xi)$ is evaluated on η_0 -line, and ξ_0 is a value of ξ , $21.7 R_{\oplus}$, for a point at $X=0$ on it. Accordingly, ε_0 is the flux tube energy content at $\xi = \xi_0$ in the near-cusp region of $0 \leq \eta \leq \eta_0$. Parameter γ is constant (in space), and it is to control the azimuthal (ξ -) dependence of ε . A set of eqs. (7)-(9) on η_0 -line is reduced to the standard form of an adiabatic equation of state, *i.e.*, $pR_b^\gamma = \text{const}$. Physical determination of γ is beyond the scope of the present study, whereas this may be involved in the problem of the formation of LLBL or the mechanism by which magnetosheath particles enter it. Fortunately, however, the FAC generation in the LLBL region is essentially attributed to the gradient of $\partial\varepsilon/\partial\eta$, not significantly affected by $\partial\varepsilon/\partial\xi$ (*i.e.*, the value of γ), so long as $\gamma \geq 0$ as assumed theoretically. This point will be discussed further in the next section. In eq. (10), $\delta\eta$ represents the characteristic length for an energy density falloff, and a and b are determined so that $g(1)=0$ and $g(\eta_0)=1$. For $\delta\eta=1/4$ (which is assumed hereafter), the function $g(\eta)$ is illustrated in Fig. 6, where $b=\tanh 2$ and $a=b-\tanh\{4 \cdot (1/32-1/2)\}$.

In the present model, the LLBL is assumed to be closed. However, whether the LLBL is on closed or open field lines have been controversial (*e.g.*, Onsager *et al.*, 1993; Moen *et al.*, 1996; Lockwood, 1997). Lockwood has predicted that the low-altitude precipitation of a mixture of magnetosheath and magnetospheric ions, as assumed to be a signature of the LLBL, can be identified in an open region in the noon sector. He did not argue, however, the entire openness of the LLBL itself at low magnetic latitudes. From direct (*in situ*) observations of the LLBL, most of the LLBL (not its ionospheric projection nor the region of particle precipitation) is inferred to be on closed field lines even when the IMF $B_z < 0$. For example, Fig. 1 of Song *et al.* (1993) shows that the number density in the boundary layer, except at its outer edge, is only a few percent of the density in the sheath transition layer (just outside of the boundary layer). This fact cannot be understood if the boundary layer is open. This is because a considerable amount of magnetosheath particles can flow along the open field lines into the boundary layer. The closed LLBL is basically in conformity with a generally accepted view that the LLBL is

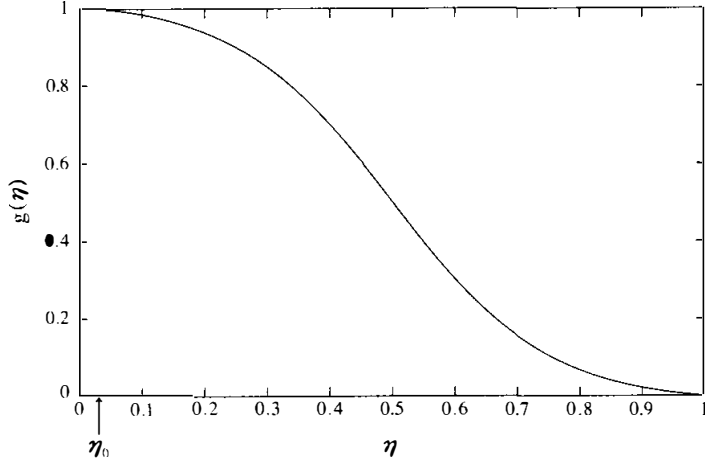


Fig. 6. Profile of $g(\eta)$ in eq. (10), where $\delta\eta = 1/4$.

formed regardless of the IMF and the occurrence of the magnetic reconnection at the dayside magnetopause. The reconnection will act to open only an outermost part of the LLBL.

3. FAC generation in LLBL

For the isotropic plasma pressure uniform along the field lines, the (quasi-steady) FAC density $J_{\parallel i}$ at the ionospheric height is given by the following equation (Yamamoto *et al.*, 1996; hereafter referred to as Y96):

$$J_{\parallel i} = e \bar{\mathbf{v}}_{m,i} \cdot \nabla_i \epsilon, \quad (11)$$

where $e (>0)$ is the electronic charge, a positive value of $J_{\parallel i}$ corresponds to an FAC flowing away from the ionosphere, *i.e.*, an upward FAC, and ∇_i denotes the gradient on the ionospheric plane. In this analysis, the ionospheric plane is assumed to be perpendicular to the ambient magnetic field \mathbf{B}_i . The velocity $\bar{\mathbf{v}}_{m,i}$ is the average of the ionospheric projection of the magnetic drift velocity per unit energy, which is defined as follows:

$$\bar{\mathbf{v}}_{m,i} \equiv \frac{1}{R_b} \int_{s_i}^{s_e} \frac{V_{m,i}(s)}{W^p} \frac{\mathbf{B}_i}{B(s)} ds, \quad (12)$$

where $V_{m,i}(s)$ is the ionospheric projection of the magnetic drift velocity of a proton fluid with average energy W^p . The velocity $\bar{\mathbf{v}}_{m,i}$ is derived from the gradient of R_b (Vasyliunas, 1970; Y96):

$$\bar{\mathbf{v}}_{m,i} = -\frac{2}{3e} \frac{1}{R_b B_i} \mathbf{b}_i \times \nabla_i R_b, \quad (13)$$

where \mathbf{b}_i is the unit vector parallel to the ionospheric magnetic field \mathbf{B}_i .

If the FAC density at the equator is defined as $J_{\parallel e} = (B_e/B_i) J_{\parallel i}$, *i.e.*, $J_{\parallel i}$ multiplied by

the mirror ratio of B_e/B_i , where $B_e = B(s_e)$, $J_{\parallel e}$ is expressed as

$$J_{\parallel e} = e(B_e/B_i)\bar{\mathbf{v}}_{m,e} \cdot \nabla_e \mathcal{E}, \quad (14)$$

where ∇_e denotes the gradient on the equatorial plane. When the field lines as well as the plasma distributions are symmetric with respect to the equator, the FAC density vanishes there. The current density $J_{\parallel e}$ is then defined only in a formal sense. The definition of $\bar{\mathbf{v}}_{m,e}$ (the average of the equatorial projection of the magnetic drift velocity per unit energy) and its relation to R_b are given by

$$\bar{\mathbf{v}}_{m,e} \equiv \frac{1}{R_b} \int_{s_i}^{s_e} \frac{V_{m,e}(s)}{W^p} \frac{B_i}{B(s)} ds, \quad (15)$$

and

$$\bar{\mathbf{v}}_{m,e} = -\frac{2}{3e} \frac{1}{R_b B_e} \mathbf{b}_e \times \nabla_e R_b, \quad (16)$$

where $V_{m,e}(s)$ is the equatorial projection of the magnetic drift velocity of a proton fluid with average energy W^p , and \mathbf{b}_e is the unit vector parallel to the equatorial magnetic field \mathbf{B}_e .

As is evident from eq. (11) or (14), the FAC direction (*i.e.*, the polarity of charge separation) is determined by the direction of $\bar{\mathbf{v}}_{m,i(e)}$ relative to that of $\nabla_{i(e)} \mathcal{E}$. The direction of $\bar{\mathbf{v}}_{m,i}$ or $\bar{\mathbf{v}}_{m,e}$ is perpendicular to $\nabla_i R_b$ or $\nabla_e R_b$, respectively (see eq. (13) or (16)). Equivalently, the averages of the magnetic drifts projected to the ionospheric or equatorial plane are parallel to the equicontours of the flux tube volume R_b plotted on one plane. (Neglecting $\nabla_{i(e)} B_i$, the stream function for $\bar{\mathbf{v}}_{m,i}$ is given by $(2/3eB_i) \ln R_b$ (Y96), but $(2/3eB_i) \ln R_b$ on the equatorial plane is the stream function for $(B_e/B_i)\bar{\mathbf{v}}_{m,e}$.) An important factor for the FAC generation is then the equicontours of R_b , which are shown, on the equatorial plane, in Fig. 7, where the inner edge of the model LLBL (Fig. 5a) is superposed, and R_b is normalized by R_{b0} , the value of R_b (1.32×10^{10} m) for the dipole field line with an equatorial distance of $7 R_E$. In contrast with the magnetic drift direction schematically illustrated in Fig. 3 of Yang *et al.* (1994), all R_b -contours in T89 are closed inside the open-closed boundary, *i.e.*, the magnetopause. Figure 8 shows the ‘distortion angles’ of division lines: the distortion angle at a point on one line is defined as the angle between $\bar{\mathbf{v}}_{m,e}$ and the tangent to it there. The distortion angle (at a given X) is greater on more inner division lines, as can be understood as a characteristic of equicontours closed inside the magnetopause. Similarly to the region I FACs on the nightside plasma sheet (Y96), the LLBL FACs are also controlled by the degree of ‘distortion’. (This point will be again discussed below). For reference, Fig. 9 shows the magnitudes of $\bar{\mathbf{v}}_{m,i} \times 1 \text{ keV}$ plotted along various division lines mapped to the ionosphere.

A remarkable feature of the R_b -contours in Fig. 7 is that some of them cross the LLBL inner edge, namely $\bar{\mathbf{v}}_{m,e}$ at the LLBL inner edge has a component normal to it. The distortion angles in Fig. 8 are a manifestation of this situation. Such a feature (for all division lines) assures the generation of a region I FAC in the whole LLBL region, when the flux tube energy content \mathcal{E} does not increase with ξ (antisunward), *i.e.*, $\gamma \geq 1$ in eq. (8). This is because in the scalar product of $\bar{\mathbf{v}}_{m,e} \cdot \nabla_e \mathcal{E}$ in eq. (14), the term of $\bar{v}_{m,e}^{\xi} \nabla_e^{\xi} \mathcal{E}$ (product of ξ -components) is zero or of the same sign as the term $\bar{v}_{m,e}^{\eta} \nabla_e^{\eta} \mathcal{E}$ (product of η -components) contributing to the generation of the region I FAC. Hereafter, $\bar{v}_{m,e}^{\xi} \nabla_e^{\xi} \mathcal{E}$ and

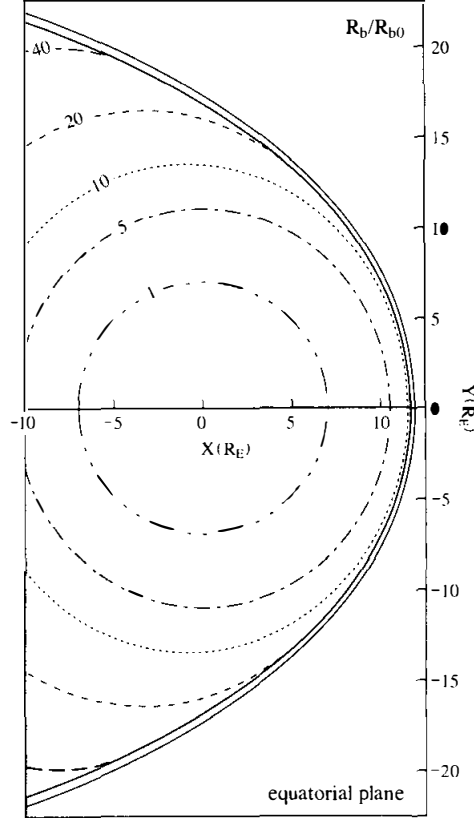


Fig. 7. Equicontours of the flux tube volume R_b normalized by R_{b0} on the equatorial plane, where R_{b0} is the value of R_b , (132×10^{10} m) for the dipole field line with an equatorial distance of $7 R_E$.

$\nabla_{m,e}^{\xi} \nabla_{e}^{\xi} \varepsilon$ are referred to as the 'perpendicular' and 'parallel' contributions to $J_{\parallel e}$, respectively. Even in the case of $\gamma < 1$, a region I FAC can be generated so long as the increase (with ξ) of ε is sufficiently slow. Since the density and temperature of the 'source' magnetosheath population are expected to decrease with ξ (or $-X$) (Spreiter *et al.*, 1966), a maximum (conceivable) gradient of $\partial \varepsilon / \partial \xi (> 0)$ might be attained when $\varepsilon \propto R_b$, which corresponds to $\gamma = 0$ in eq. (8). For that case (the result not shown), the region I current intensity for $\xi \lesssim 10$ is relatively small, but the intensity at $\xi = \xi_0$ is about 63% of that in the case of $\gamma = 5/3$ and the total current, *i.e.*, the intensity integrated down to the adiabatic limit (for details, see below) is more than that for $\gamma \geq 1$. Therefore, almost unconditionally (only if $\gamma \geq 0$), upward FACs are generated from the postnoon LLBL, implying the production of negative space charges. Similarly, downward FACs are from the prenoon LLBL, producing positive ones.

In passing, expressions for the FAC intensity and the total current are obtained for the situation that the perpendicular contribution to $J_{\parallel e}$ dominates the parallel one. In this case, combination of eqs. (14) and (16) yields

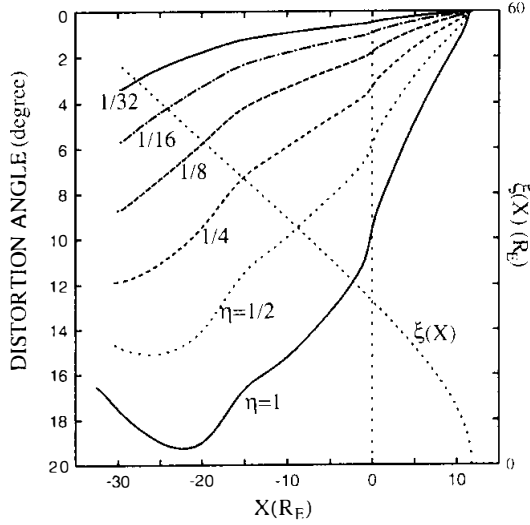


Fig. 8. Distortion angles of division lines at $\eta = 1, 1/2, 1/4, 1/8, 1/16$ and $1/32$, plotted against X . (For the definition of distortion angle, see Section 3.) Also $\xi(X)$ is plotted with the ordinate on the right.

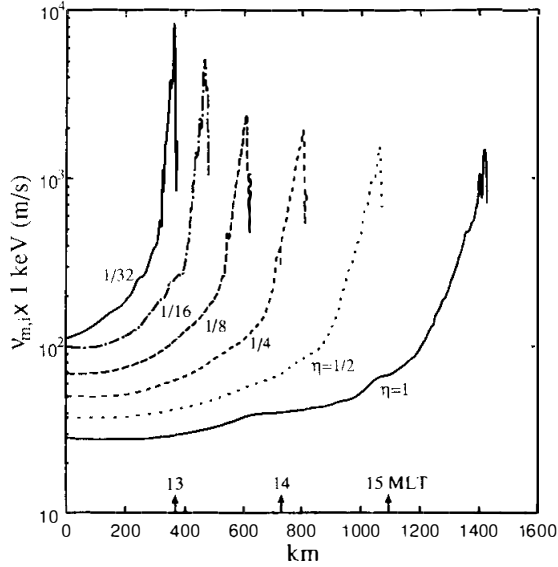


Fig. 9. Magnitudes of $\bar{v}_{m,i} \times 1 \text{ keV}$ plotted along various division lines mapped to the ionosphere. The abscissa is the distance (in km) from noon. The MLT on 1.0 line is indicated on the abscissa.

$$J_{\parallel e} = \pm \frac{2}{3B_i} \frac{1}{R_b} \frac{\partial R_b}{\partial \xi} \frac{\partial \varepsilon}{\partial(\eta \Delta)}, \quad (17)$$

where the plus and minus signs are for $J_{\parallel e}$ on the morning and evening sides, respectively.

Integrating the above equation along the η -axis gives the current intensity, $I_e(\xi)$, in the LLBL. Since $\partial \ln R_b / \partial \xi$ is nearly independent of η , $I_e(\xi)$ is approximately written as

$$I_e'(\xi) \sim \mp \frac{2}{3B_i} \varepsilon(\xi, \eta_0) \left[\frac{\partial \ln R_b}{\partial \xi} \right]_{\eta=1/2}. \quad (18)$$

Integrating again the above equation along the ξ -axis gives the total current, I_e^0 :

$$I_e^0 \sim \mp \frac{2}{3B_i} \int_0^{\xi_n} d\xi \varepsilon(\xi, \eta_0) \left[\frac{\partial \ln R_b}{\partial \xi} \right]_{\eta=1/2} \quad (19)$$

This integration is from the subsolar point to a point (ξ_n, η_0) where the adiabaticity parameter (Büchner and Zelenyi, 1989), κ , is equal to unity. Here κ^2 is the ratio between the radius of the field-line curvature and the Larmor radius of a proton with 1 keV of energy. In a distant tail region of $\xi > \xi_n$, the proton motion is assumed nonadiabatic, *i.e.*, the drift approximation breaks down. Paying attention to the bracketed part of the integrand in eq. (19), which depends directly on the field distribution, I_e^0 is found to be proportional to

$$\left[\ln \frac{R_b(\xi_n)}{R_b(0)} \right]_{\eta=1/2}. \quad (20)$$

Analogous to the case of the generation of a nightside region I FAC (Yamamoto *et al.*, 2001), quantity (20) is assumed to represent the degree of the magnetic field distortion in the LLBL. The LLBL region I current thus depends on the field distortion.

Regarding the causality underlying the generation of LLBL FACs, the following two possibilities are suggested. The generation of LLBL FACs may be an inevitable result of the formation of the magnetopause confining the R_b -contours on the equatorial plane, which would otherwise be distributed in a (dipole-)axially symmetric manner. Note that the magnetopause currents act to shield the magnetospheric fields so that all R_b -contours can be closed inside the open-closed boundary (see Fig. 7) where R_b increases indefinitely. A second possibility is that the ultimate cause of the LLBL FAC generation is the solar wind distortion of the terrestrial magnetic field lines which would be configured symmetrically (in the same sense as described above) without the influence of the solar wind; more simply, the LLBL FAC generation is attributed ultimately to the loss of field line symmetry.

4. Numerical results

The FAC density and intensity in the LLBL region are numerically calculated using eq. (14) for the distributions of ε in eqs. (7)–(10) and $\bar{\nu}_{m,e}$ based on the T89 field. At a point (ξ_0, η_0) , the plasma density, n_0 , is assumed to be 1.0 cm^{-3} , and the total average energy, $W_0 \equiv W^p + W^e$, is 0.5 keV. The energy content ε_0 is then estimated as $n_0 W_0 R_b(\xi_0, \eta_0)$, where $R_b(\xi_0, \eta_0)$ is about $36.9 R_{b0}$. It is straightforward to obtain the FAC density/intensity for other values of parameters n_0 and W_0 , because of its proportionality to these parameters. Parameter γ is taken to be 5/3 unless otherwise stated.

Figure 10 shows equicontours of the FAC density $J_{\parallel i}$ on the ionosphere. Figure 11a shows the current intensities in the LLBL, nearcusp and whole regions, defined as

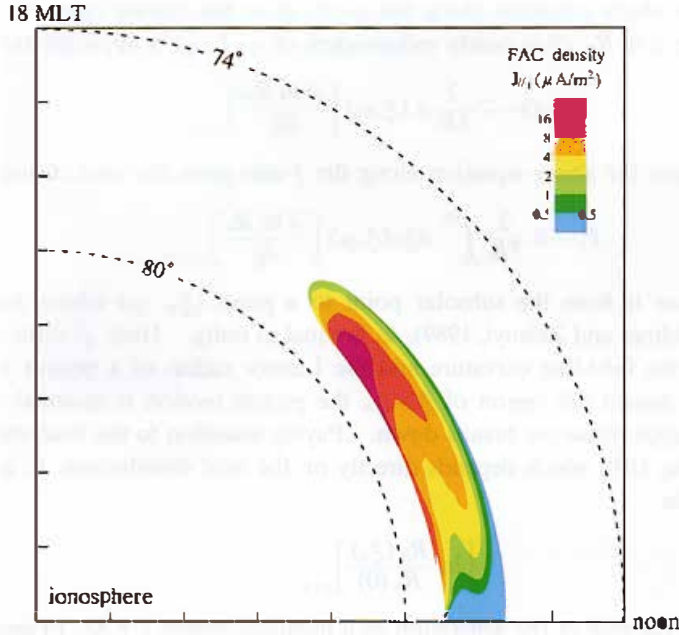


Fig. 10. Equiconours of FAC density J_{FAC} on the ionosphere for the flux tube energy content ε in eqs. (7)–(10) with $\gamma=5/3$, $\partial\eta=1/4$ and $\varepsilon_0=n_0W_0R_0(\xi_0, \eta_0)=1.0 \times 0.5$ (keV cm^{-1}) $\times 36.9 R_0$. The color bar indicates the FAC density ($\mu\text{A/m}^2$).

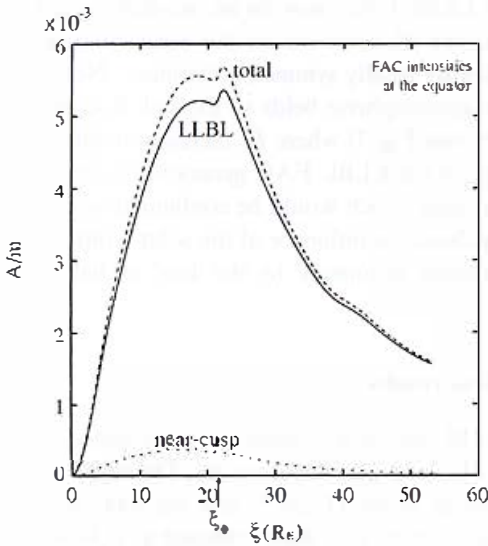


Fig. 11a

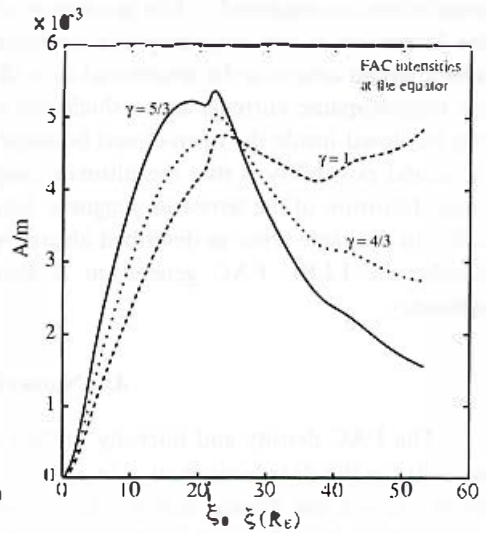


Fig. 11b

Figs 11a, b. (a) Current intensities in the LLBL, near-cusp and whole regions (For the definitions of these regions, see Section 3.) (b) Current intensity in the LLBL for $\gamma=5/3, 4/3$ and 1. In (a)–(c) the ξ -coordinate is given on the abscissas and the position of ξ_0 (corresponding to $X=0$) is indicated; γ is 5/3 in (a) and (c).

$\int_{\eta_0}^1 J_{\perp e} \Delta d\eta$, $\int_0^{\eta_0} J_{\perp e} \Delta d\eta$ and $\int_0^1 J_{\parallel e} \Delta d\eta$, respectively. Figure 11b shows the current intensity in the LLBL for $\gamma = 5/3, 4/3$ and 1.0. In Fig. 11c, the FAC densities $J_{\parallel e}(\xi, \eta)$ on various division lines, at the equator, are plotted against ξ ; the perpendicular and parallel contributions to $J_{\perp e}$ (i.e., $\bar{v}_{m,e}^{\eta} \nabla_{\xi}^{\eta} \varepsilon$ and $\bar{v}_{m,e}^{\xi} \nabla_{\eta}^{\xi} \varepsilon$) are also shown.

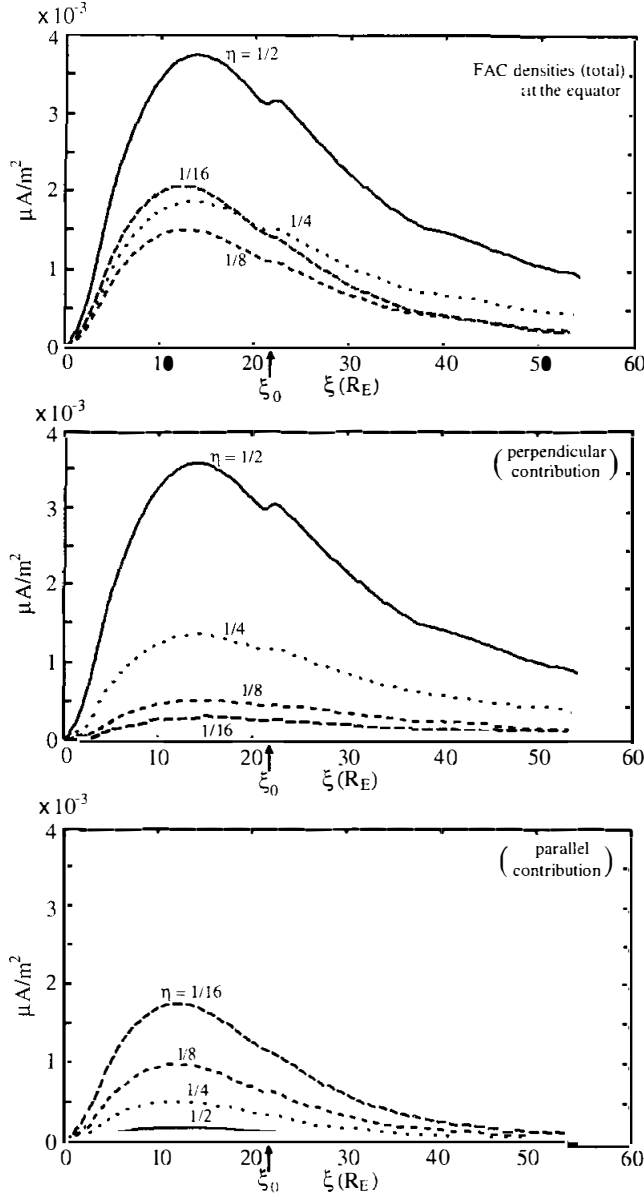


Fig. 11c. Current density $J_{\perp e}(\xi, \eta)$ on various division lines at the equator; perpendicular and parallel contributions to $J_{\perp e}$ (defined in Section 3) are also shown.

From Fig. 10 it is found that the region 1 currents around 14–15 (or 9–10) MLT have large values of $|J_{\parallel}|$ (e.g., $> 8 \mu\text{A}/\text{m}^2$) in wider latitudinal ranges, being consistent with the statistical distribution of J_{\parallel} in Fig. 14 of Iijima and Potemra (1978). Figure 11a indicates that in the case of $\gamma=5/3$, the region 1 current intensity in the LLBL is relatively large in a region around $X=0$ (i.e., $\xi=\xi_0=21.7 R_E$). For smaller values of $\gamma (\geq 1)$, the intensity distribution becomes broader in ξ (see Fig. 11b), because ε decreases more slowly with ξ or does not decrease. It is found that in the case of $\gamma=5/3$, the perpendicular contribution to $J_{\parallel e}$ dominates the parallel one in a wide η -range of $\eta > 1/4$ (see Fig. 11c). For smaller values of $\gamma (\geq 1)$, the parallel contribution becomes smaller because of smaller values of $\partial\varepsilon/\partial\xi$; particularly it vanishes for $\gamma=1$.

Finally the K_p -dependence of the region 1 FAC in the LLBL is briefly discussed. Numerical calculations show that the average current intensity defined as I_e^0/ξ_n as well as the distortion degree, (20), are insensitive to K_p . (More exactly, they are not systematically changed with K_p .) On the other hand, the observations from the TRIAD satellite (Iijima and Potemra, 1982) have shown that the average densities of the dayside region 1 current increase with the magnitude of southward IMF component, and are better correlated with $P_{\text{dyn}}^{1/4} (B \sin(\theta/2))^{1/2}$, where P_{dyn} is the solar wind dynamic pressure, B the IMF strength, and θ the IMF clock angle. This fact may be explained by the fact that magnetosheath particles can be energized, depending on the interplanetary electric and magnetic fields, on the frontside magnetopause just before entering the LLBL region. This issue will be studied in a subsequent paper.

5. Variations of LLBL FAC structure

While the current structure as modelled in the previous sections is assumed to represent, in a sense, a statistically averaged one, satellite observations have shown a variety of the region 1 current structures such as a thin current sheet, multiple current sheets and a broad current zone. In this section, possible physical processes to control the thickness of a current zone (in the LLBL region) are briefly discussed.

5.1. Preconditions for a thin current sheet

As is discussed in Section 1, the DE-I magnetic field data sometimes show the appearance of an apparently single current sheet which is localized in a narrow ($< 0.5^\circ$ in invariant latitude) zone, but can substantially maintain the total region 1 current intensity on a latitudinal line crossing the LLBL region. Here, an attempt is made to identify a specific physical condition required for such a current sheet to emerge. Figure 4b shows variations of the IMF GSM components as well as the solar wind speed, density and dynamic pressure, which were measured by the IMP 8 satellite for a four-hour period just prior to the DE-I observation of the current structure in Fig. 4a. Remarkably, every quantity in Fig. 4b remains at a nearly constant level. An example of the appearance of a thin current sheet under steady solar wind conditions can be found in the previously published literature: the magnetic field and plasma data from the DE-I in Fig. 2 of Burch *et al.* (1983) shows the existence of a downward region 1 current having width of about 0.3° in invariant latitude in the prenoon LLBL region. The ISEE 3 data shows that solar wind parameters had been nearly steady for several hours before this DE-I observation,

although there are some data gaps. These observations suggest that a steady state of the solar wind may be one precondition for the formation of a thin region 1 current sheet in the LLBL. Note that a thin current sheet does not always appear in steady solar wind conditions, probably because of plasma instabilities in the magnetosphere.

Since the average location of the magnetopause is controlled by the IMF as well as the solar wind dynamic pressure (e.g., Roelof and Sibeck, 1993; Fairfield, 1995; Petrinec and Russell, 1996; Shue *et al.*, 1997), variations of the solar wind parameters will cause the magnetopause to move or oscillate. The following sections describe how the magnetopause oscillation influences the spatial structure of the LLBL region 1 current.

5.2. Thickening of a region 1 current zone

The satellite observations of hot boundary layer plasmas (Sckopke *et al.*, 1981; Lundin and Evans, 1985) have indicated that an injected magnetosheath plasma is embedded in a "halo" of magnetospheric plasma. This structure is schematically shown in Fig. 12a, adapted from Fig. 7 of Sckopke *et al.* The energy-dependent magnetic drifts of the injected hot particles act to smooth out, in the azimuthal direction, the wavy structure, making the injection boundary of the magnetosheath plasma diffusive. More precisely, even a plasma of the boundary layer proper is thought to be a mixture of plasma sheet and magnetosheath populations: probably, a microscopic filament of sheath particles injected, by a (locally enhanced) $E \times B$ drift, into the magnetosphere will merge with the already mixed plasma, due to the magnetic drift and field-aligned motions. This picture is consistent with the observations that particle energy spectra obtained in respective regions of the magnetosheath, outer boundary layer, inner boundary layer and plasma sheet all

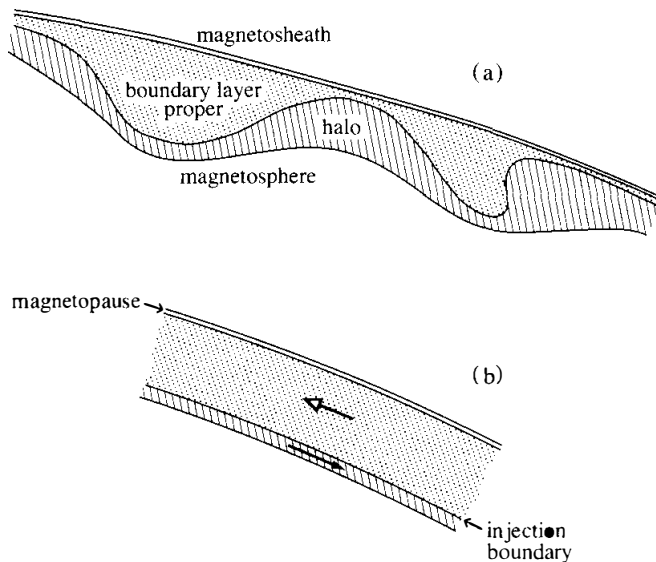


Fig. 12. (a) Schematic illustration of boundary layer plasmas based on the ISEE 1 and 2 satellite observations by Sckopke *et al.* (1981). (b) Simple model of the injection boundary, roughly parallel to the magnetopause boundary. The open- and closed-headed arrows denote antisunward and sunward plasma flows, respectively.

cross at approximately one point (*e.g.*, Eastman *et al.*, 1976; Song *et al.*, 1990; Traver *et al.*, 1991).

To consider the effect of the magnetopause fluctuation on the region 1 current structure rather than the aforementioned azimuthal 'diffusion' effect, suppose such a laminar structure of the LLBL plasma as shown in Fig. 12b, where the injection boundary is roughly parallel to the magnetopause boundary. When the magnetopause stands still (as tentatively assumed), the distance between the injection boundary and the magnetopause represents (in an average sense) the inherent penetration depth of magnetosheath particles. Then, the injection boundary for the stationary magnetopause is hereafter referred to as the penetration limit of the magnetosheath plasma. (As will be discussed below, the actual injection boundary for the magnetopause in motion is different from the penetration limit.) In the situation in Fig. 12b, as predicted from the theory in Section 3, the region 1 current will arise near the penetration limit, provided that the boundary layer proper is crosswise-uniform. The penetration limit is sharp, but it is assumed to have a finite thickness (of the order of $\sim 0.1^\circ$ in footpoint latitude), which also gives the minimum thickness of the region 1 current zone. Associated space charges emerge in the region 1 current zone, so that the stagnation line (where the convection flow ceases) appears inside the current zone, because the intensity of the region 2 current is usually smaller than that of the region 1 current. The observations (*e.g.*, Sckopke *et al.*, 1981) have shown that the antisunward flow speed in the region of injected magnetosheath often exceeds 100 km/s, but in other regions the flow speeds are on the order of 10 km/s. The above picture of the LLBL may hold true for the case of the southward IMF, but during periods of northward IMF, the convection flow associated with the NBZ field-aligned currents (Iijima *et al.*, 1984; Iijima and Shibaji, 1987) could act to transport the magnetosheath plasma deeper into the magnetosphere, thereby thickening the LLBL (see observations by Mitchell *et al.*, 1987). Hence the following discussion will be focused on the southward IMF case.

A practical point is to what extent a displacement of the magnetopause can change the ionospheric footpoints of field lines threading the penetration limit of a magnetosheath plasma. The T89 model is used to assess the relation in displacement between the magnetopause and the footprint of the penetration limit. To obtain a displaced magnetopause (defined as the open-closed boundary), a magnetic field (of magnitude of a few nanoTeslas) in the Z-direction is uniformly added to the T89 field. The penetration limit is assumed to be one of the division lines in the model LLBL region, which are defined in Section 2. Taking 0.6 (division) line or 1.0 line as the penetration limit, Fig. 13 shows the ratio of the displacement of the penetration limit footprint to the magnetopause displacement, plotted against MLT (defined on the ionosphere), where the magnetopause displacement is in units of the Earth's radius and the footprint displacement is in units of the distance of one degree latitude, *i.e.*, about 110 km. The displacement of the magnetopause boundary at a point (on the original boundary) is defined, on the equatorial plane, as the minimum distance from the point to the displaced one, and the footprint displacement is defined similarly on the ionospheric plane.

An examination of ISEE 1 and 2 data during intervals of multiple magnetopause crossings (Song *et al.*, 1988) has shown that the average peak-to-peak amplitude of magnetopause oscillations is about $0.5 R_E$ under southward IMF conditions, for oscillation periods from ~ 2 to ~ 30 min. From Fig. 13, it is then inferred that observed

Fig. 13. Ratio of the displacement of the penetration limit footprint to the magnetopause displacement, plotted against MLT (defined on the ionosphere); the penetration limit is taken to be 1.0 line (LLBL inner edge) or 0.6 line. The magnetopause displacement is in units of the Earth's radius, and the footprint displacements are in units of the distance of one degree latitude, i.e., about 110 km. (For the definitions of these displacements, see Section 5.2.)

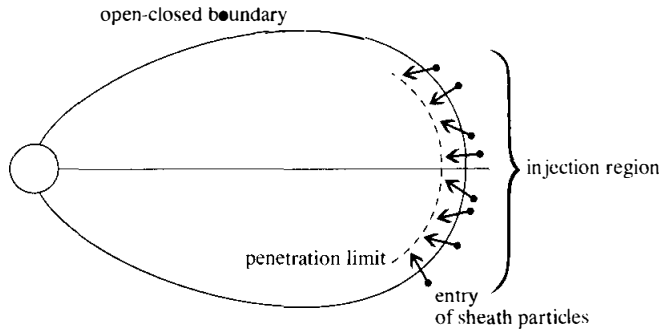
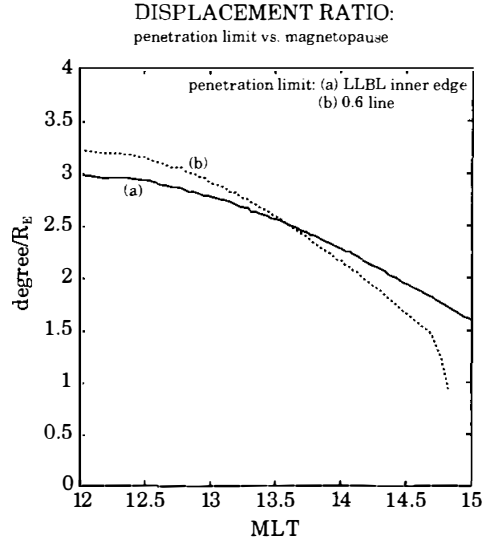


Fig. 14. Schematic illustration of the injection of magnetosheath particles into the LLBL.

magnetopause oscillations may fluctuate the ionospheric footprint of the penetration limit, with an amplitude of roughly one degree. Here suppose an azimuthally convecting flux tube carrying plasma particles together with field lines threading the LLBL. When the flux tube happens to be within the (instantaneous) penetration limit, in the course of magnetopause oscillations, it will be intruded, at low-latitudes, by newly injected magnetosheath particles (see Fig. 14). When it is earthward of the penetration limit, it will not be subject to such intrusion. The particle distribution in the flux tube close to the average penetration limit can be affected by intermittent loading of magnetosheath particles, if the magnetopause oscillation period is shorter than the time required for the plasma tube to travel over a distance of $\approx 10 R_E$ (a significant fraction of the total length of the LLBL bounded by the adiabaticity limit (see Section 3)). For example, the particle distribution in a flux tube in a stagnant plasma with a speed of 20 km/s will be affected by oscillations with periods shorter than 50 min, while a plasma tube with a high speed of 200 km/s will

be affected only by oscillations with periods less than 5 min. (Either of these period ranges falls within the aforementioned range for the actual observation.) Thus, the magnetopause oscillations as observed by Song *et al.* could lead to the formation of a transition layer in which the content of a flux tube changes from being highly abundant in magnetosheath particles to lacking in them. From the results shown in Fig. 13 and the findings of Song *et al.*, the ionospheric thickness of this transition layer is inferred to be roughly one degree in latitude. As can be seen from eq. (11), this also gives the width of the (thickened) region 1 current under the influence of magnetopause oscillations.

The above estimation of the width of the region 1 current is somewhat speculative. A more convincing evaluation of this thickening effect would require a numerical simulation for the oscillating magnetopause with a realistically modelled LLBL; this task will be attempted in the future.

5.3. Effect of latitudinal convection

An effect of $E \times B$ convection on the latitudinal width of the region 1 current is briefly considered here. This is just the velocity filter effect. For simplicity, suppose such a simple structure of the LLBL as illustrated in Fig. 12b. Since the low-latitude portion of a flux tube in the LLBL region is intruded by sheath particles (see Fig. 14), it takes some time for them to travel along the field lines to low altitudes. If the average field-aligned speeds of injected ions are in the range between 100 and 400 km/s, it takes 160–640 s to travel over a distance of 10 R_E . In such time intervals, the sheath particles are convected poleward, under southward or weakly northward IMF conditions. Therefore, under the assumption that the convection speed has a latitudinal component of 0.1 km/s as viewed on the ionosphere, the inner (equatorward) edge of the population of injected sheath ions just above the ionosphere has a width of roughly 0.5° in latitude, even if the inner edge of the low-latitude (near the equator) portion of that population is strictly sharp. Basically, the FAC width is controlled by the characteristic scale length for a gradient of the flux tube energy content (see eq. (11)). Also noting that the cross section of a flux tube as well as the magnetic drift are greater in magnitude at higher altitudes, particularly in a region near the equator, the LLBL FAC width, under the influence of latitudinal convection, is then estimated as at most $\approx 0.5^\circ$ in latitude, although it may depend on the convection speed, the energy distribution of LLBL ions, the field line length, and so on.

At the same time, the velocity filter effect may alter the spatial relation between the inner edge of the precipitating LLBL ions and the associated FAC region. Particularly at low altitudes, the former can be shifted poleward from the latter due to that effect. Such a signature may be discernible in high spatial resolution data of currents and particles. In the Viking observation in Fig. 2, the equatorward edge of LLBL ion precipitation is located slightly poleward of the region of intense downward current. In this case, data of the IMF is not available, but it is inferred to be southward from $K_p = 5^+$.

6. Conclusions

It has been shown that region 1 FACs are inevitably produced in the LLBL region by the pressure-gradient-driven mechanism, whenever magnetosheath particles enter that region. The current density/intensity distributions numerically evaluated for a plausible

profile of the LLBL particle population in the framework of the 1989 Tsyganenko model are consistent with observations. This FAC generation is ultimately attributed to the magnetic field distortion in the LLBL region, namely a property of the flux tube volume that it changes significantly along the LLBL inner edge.

Acknowledgments

The work of T. Yamamoto was supported in part by the joint research programs at Radio Atmospheric Science Center, Kyoto University, Uji, Kyoto and the National Institute of Polar Research, Itabashi, Tokyo. The DE-1 6-s average magnetometer data and IMP 8 15-s average data were obtained from the NSSDC SPyCAT data distribution sites (Dieter K. Bilitza and Joseph H. King, respectively). The 5-min averages of solar wind parameters were from the NSSDC IMP 8 Magnetometer Data Server (H. Bridge, A. J. Lazarus, S.M. Petriner and C.T. Russell).

The editor thanks the referees for their help in evaluating this paper.

References

- Axford, W.I. and Hines, C.O. (1961): A unifying theory of high-latitude geophysical phenomena and geomagnetic storms. *Can. J. Phys.*, **39**, 1433-1464.
- Burch, J.L., Reiff, P.H. and Sugiura, M. (1983): Upward electron beams measured by DE-1: a primary source of dayside region-1 Birkeland currents. *Geophys. Res. Lett.*, **10**, 753-756.
- Büchner, J., and Zelenyi, L.M. (1989): Regular and chaotic charged particle motion in magnetotaillike field reversals I. Basic theory of trapped motion. *J. Geophys. Res.*, **94**, 11821-11842.
- Bythrow, P.F., Heelis, R.A., Hanson, W.B. and Power, R.A. (1981): Observational evidence for a boundary layer source of dayside region 1 field-aligned currents. *J. Geophys. Res.*, **86**, 5577-5589.
- Bythrow, P.F., Potemra, T.A., Zanetti, L.J., Erlandson, R.E., Hardy, D.A., Rich, F.J. and Acuna, M.H. (1987): High latitude currents in the 0600 to 0900 MLT sector: observations from Viking and DMSP-F7. *Geophys. Res. Lett.*, **14**, 423-426.
- Bythrow, P.F., Potemra, T.A., Erlandson, R.E. and Zanetti, L.J. (1988): Birkeland currents and charged particles in the high-latitude prenoon region: A new interpretation. *J. Geophys. Res.*, **93**, 9791-9803.
- Eastman, T.E., Hones, E.W., Jr., Bame, S.J. and Asbridge, J.R. (1976): The magnetospheric boundary layer: Site of plasma, momentum and energy transfer from the magnetosheath into the magnetosphere. *Geophys. Res. Lett.*, **3**, 685-688.
- Erlandson, R.E., Zanetti, L.J., Potemra, T.A., Bythrow, P.H. and Lundin, R. (1988): IMF B_y dependence of region 1 Birkeland currents near noon. *J. Geophys. Res.*, **93**, 9804-9814.
- Fairfield, D.H. (1995): Observations of the shape and location of the magnetopause: A review. *Physics of the Magnetopause*, ed. by P. Song *et al.* Washington, D.C., Am. Geophys. Union, 53-60 (*Geophys. Monogr.*, 90).
- Friis-Christensen, E. and Lassen, K. (1991): Large-scale distribution of discrete auroras and field-aligned currents. *Auroral Physics*, ed. by C.-I. Meng *et al.* New York, Cambridge Univ. Press, 369-381.
- Gurgiolo, C. and Burch, J.L. (1982): DE-1 observations of the polar wind—A heated and unheated component. *Geophys. Res. Lett.*, **9**, 945-948.
- Iijima, T. and Potemra, T.A. (1978): Large-scale characteristics of field-aligned currents associated with substorms. *J. Geophys. Res.*, **83**, 599-615.
- Iijima, T. and Potemra, T.A. (1982): The relationship between interplanetary quantities and Birkeland

- current densities. *Geophys. Res. Lett.*, **9**, 442-445.
- Iijima, T., Potemra, T.A., Zanetti, L.J. and Bythrow, P.F. (1984): Large-scale Birkeland currents in the dayside polar region during strongly northward IMF: A new Birkeland current system. *J. Geophys. Res.*, **89**, 7441-7452.
- Iijima, T. and Shibaji, T. (1987): Global characteristics of northward IMF-associated (NBZ) field-aligned currents. *J. Geophys. Res.*, **92**, 2408-2424.
- Kaufmann, R.L., Larson, D.J., Beidl, P. and Lu, C. (1993): Mapping and energization in the magnetotail. *J. Geophys. Res.*, **98**, 9307-9320.
- Liou, K., Newell, P.T., Meng, C.I., Sotirelis, T., Brittnacher, M., and Parks, G. (1999): Source region of 1500 MLT auroral bright spots: simultaneous polar UV-images and DMSP particle data. *J. Geophys. Res.*, **104**, 24587-24602.
- Lockwood, M. (1997): Relationship of dayside auroral precipitations to the open-closed separatrix and the pattern of convective flow. *J. Geophys. Res.*, **102**, 17475-17487.
- Lotko, W. and Sonnerup, B.U.Ö. (1995): The low-latitude boundary layer on closed field lines. *Physics of the Magnetopause*, ed. by P. Song *et al.* Washington, D.C., Am. Geophys. Union, 371-383 (*Geophys. Monogr.*, 90).
- Lotko, W., Sonnerup, B.U.Ö. and Lysak, R.L. (1987): Nonsteady boundary layer flow including ionospheric drag and parallel electric fields. *J. Geophys. Res.*, **92**, 8635-8648.
- Lundin, R. and Evans, D.S. (1985): Boundary layer plasmas as a source for high-latitude, early afternoon, auroral arcs. *Planet. Space Sci.*, **32**, 1389-1406.
- Mitchell, D.G., Kutchko, F., Williams, D.J., Eastman, T.E., Frank, L.A. and Russell, C.T. (1987): An extended study of the low-latitude boundary layer on the dawn and dusk flanks of the magnetosphere. *J. Geophys. Res.*, **92**, 7394-7404.
- Moen, J., Evans, D., Carlson, H.C. and Lockwood, M. (1996): Dayside moving auroral transients related to LLBL dynamics. *Geophys. Res. Lett.*, **23**, 3247-3250.
- Newell, P.T. and Meng, C.-I. (1994): Ionospheric projections of magnetospheric regions under low and high solar wind pressure conditions. *J. Geophys. Res.*, **99**, 273-286.
- Newell, P.T., Burke, W.J., Sanchez, E.R., Meng, C.-I., Greenspan, M.E. and Clauer, C.R. (1991): The low-latitude boundary layer and the boundary plasma sheet at low altitude prenoon precipitation regions and convection reversal boundaries. *J. Geophys. Res.*, **96**, 21013-21023.
- Onsager, T.G., Kleitzing, C.A., Austin, J.B. and MacKiernan, H. (1993): Model of magnetosheath plasma in the magnetosphere: cusp and mantle particles at low-altitude. *Geophys. Res. Lett.*, **20**, 479-482.
- Petrinec, S.M. and Russell, C.T. (1996): Near-Earth magnetotail shape and size as determined from the magnetopause flaring angle. *J. Geophys. Res.*, **101**, 137-152.
- Potemra, T.A., Zanetti, L.J., Erlandson, R.E., Bythrow, P.F., Gustafsson, G., Acuna, M.H. and Lundin, R. (1987): Observations of large-scale Birkeland currents with Viking. *Geophys. Res. Lett.*, **14**, 419-422.
- Roelof, E.C. and Sibeck, D.G. (1993): Magnetopause shape as a bivariate function of interplanetary magnetic field B_z and solar wind dynamic pressure. *J. Geophys. Res.*, **98**, 21421-21450.
- Sckopke, N., Paschmann, G., Haerendel, G., Sonnerup, B.U.Ö., Bame, S.J., Frbes, T.G., Hones, E.W., Jr. and Russell, C.T. (1981): Structure of the low-latitude boundary layer. *J. Geophys. Res.*, **86**, 2099-2110.
- Shue, J.-H., Chao, J.K., Fu, H.C., Russell, C.T., Song, P., Khurana, K.K. and Singer, H.J. (1997): A new functional form to study the solar wind control of the magnetopause size and shape. *J. Geophys. Res.*, **102**, 9497-9511.
- Song, P., Elphic, R.C. and Russell, C.T. (1988): ISEE 1 & 2 observations of the oscillating magnetopause. *Geophys. Res. Lett.*, **15**, 744-747.
- Song, P., Elphic, R.C., Russell, C.T., Gosling, J.T. and Cattell, C.A. (1990): Structure and properties of the subsolar magnetopause for northward IMF: ISEE observations. *J. Geophys. Res.*, **95**, 6375-6387.
- Song, P., Russell, C.T. and Huang, C.Y. (1993): Wave properties near the subsolar magnetopause: Pc

- I waves in the sheath transition layer. *J. Geophys. Res.*, **98**, 5907--5923.
- Sonnerup, B.U.Ö. (1980): Theory of the low-latitude boundary layer. *J. Geophys. Res.*, **85**, 2017-2026.
- Spreiter, J.R., Summers, A.L. and Alksne, A.Y. (1966): Hydromagnetic flow around the magnetosphere. *Planet. Space Sci.*, **14**, 223-253.
- Taguchi, S., Sugiura, M., Winningham, J.D. and Slavin, J.A. (1993): Characterization of the IMF B_z dependent field-aligned currents in the cleft region based on DE 2 observations. *J. Geophys. Res.*, **98**, 1393-1407.
- Traver, D.P., Mitchell, D.G., Williams, D.J., Frank, L.A. and Huang, C.Y. (1991): Two encounters with the flank low-latitude boundary layer: Further evidence for closed field topology and investigation of the internal structure. *J. Geophys. Res.*, **96**, 21025-21035.
- Tsyganenko, N.A. (1989): A magnetospheric magnetic field model with a warped tail current sheet. *Planet. Space Sci.*, **37**, 5-20.
- Vasyliunas, V.M. (1970): Mathematical models of magnetospheric convection and its coupling to the ionosphere. *Particles and Fields in the Magnetosphere*, ed. by B.M. McCormac. Norwell, D. Reidel, 60-71.
- Woch, J. and Lundin, R. (1993): The low-latitude boundary layer at mid-altitudes: Identification based on Viking hot plasma data. *Geophys. Res. Lett.*, **20**, 979-982.
- Woch, J., Yamauchi, M., Lundin, R., Potemra, T.A. and Zanetti, L.J. (1993): The low-latitude boundary layer at mid-altitudes: Relation to large-scale Birkeland currents. *Geophys. Res. Lett.*, **20**, 2251-2254.
- Yamamoto, T., Inoue, S. and Nishitani, N. (1995): Pressure-gradient-driven fieldaligned current at the low-latitude boundary layer (abstracts). Paper presented at the 97th Meeting of the Soc. of Geomagnetism and Earth, Planetary and Space Sciences, Nihon Univ., Tokyo, March 27-30.
- Yamamoto, T., Inoue, S., Nishitani, N., Ozaki, M. and Meng, C.-I. (1996): A theory for generation of the paired region 1 and region 2 field-aligned currents. *J. Geophys. Res.*, **101**, 27199-27222.
- Yamamoto, T., Inoue, S. and Ozaki, M. (1999): Latitudinal structure of the nightside region 1 field-aligned current observed from the EXOS-D satellite. *Adv. Polar Upper Atmos. Res.*, **13**, 105-118.
- Yamamoto, T., Inoue, S. and Ozaki, M. (2001): Distortion of the nightside boundary of the "firmly-closed" region in the 1996 Tsyganenko magnetic field model. *Adv. Polar Upper Atmos. Res.*, **15**, 43-60.
- Yamauchi, M., Lundin, R. and Woch, J. (1993): The interplanetary magnetic field B_z effects on large-scale field-aligned currents near local noon: Contributions from cusp part and noncusp part. *J. Geophys. Res.*, **98**, 5761-5767.
- Yang, Y.S., Spiro, R.W. and Wolf, R.A. (1994): Generation of region 1 current by magnetospheric pressure gradients. *J. Geophys. Res.*, **99**, 223-234.

(Received December 12, 2001; Revised manuscript accepted April 30, 2002)